Proceedings of the 2000 Winter Simulation Conference
J. A. Joines, R. R. Barton, K. Kang, and P. A. Fishwick, eds.

DEVELOPMENT OF A FAST ALL-SEASONS MODEL FOR THE STATE OF THE GROUND

Mary Albert
George Koenig

Cold Regions Research and Engineering Laboratory
U.S. Army Engineer Research and Development Center
72 Lyme Road
Hanover, NH 03755-1290, U.S.A.

George Mason

Geotechnical Laboratory
U.S. Army Engineer Research and Development Center
3909 Halls Ferry Road
Vicksburg, MS 39180-6199, U.S.A.

ABSTRACT

For predicting soil conditions in support of mobility, combat, or engineering simulations, it is important to have verified models that can reliably predict the state of the ground in all weather conditions. While variations in the state of the ground in summer are due primarily to soil type, vegetation, and slope, the winter and spring seasons present additional challenges that are currently not addressed by most Army models. Because the depth of snow on the ground varies greatly through the winter, a prediction capability is needed for the rate of snow accumulation and melt that will allow predictions of snow depth. Ground freezing/thawing or the presence of mud can significantly change soil strength, requiring a prediction capability for soil moisture and freeze/thaw. This paper describes progress in the development of FASST, the Fast All-Seasons Soil STate model. FASST is a physically based model currently under development to predict the state of the ground using minimal computational time and resources. FASST predicts soil moisture, snow depth, frost depth, snowpack melt outflow, soil temperature, and soil strength on an hourly basis. The physical basis of the model is presented, and preliminary model predictions are compared to measured field data.

1 INTRODUCTION

For a wide variety of military and civil applications, ranging from mobility prediction to agricultural or transportation problems, it is necessary to be able to predict the state of the ground under changing meteorological conditions. It is also desirable to be able to do this using modest computational resources (e.g., a PC) and modest input requirements. The purpose of this paper is to present progress in the development of such a computer model, FASST, and to present preliminary comparisons with measured field data.

Soil strength is primarily a function of the soil type, moisture content, and state (i.e. frozen or unfrozen). In cold environments, soil strength can be greatly enhanced if the soil moisture is frozen. All soils have higher bearing strength when frozen, which is manifest as an increase in the soil's cone index (CI). If the unfrozen soil has a low bearing strength, then when frozen, its CI can be significantly higher, which may have major consequences for mobility. In contrast, a layer of thawed soil (wet, low bearing strength) overlying a relatively thick frozen layer more likely has a negative impact on mobility as motion resistance increases and traction decreases with a high-moisture-content thaw layer. The thicker the wet, thawed layer, the more detrimental to mobility; the thicker the frozen layer, the more beneficial. In addition, the possibility of a snow cover will impact winter mobility.

FASST is composed of several modules that predict the state of the ground (snow depth, soil strength, soil temperature, and the state of the soil moisture) based on soil type and meteorological conditions. The net solar and infrared radiation parameters are major components of the surface energy budget model that predicts the state of the ground. These parameters are not available from standard meteorological observations. Therefore, models have been developed to predict both the net solar and infrared radiation at the surface. The freezing/thawing of the ground and the soil moisture content during thawing are very dependent on the snow depth and snowmelt outflow. A computationally fast, physically based model has been developed to predict both the snow depth and snowmelt outflow. The following sections briefly describe the main modules of the FASST model and present some preliminary results.

2 NET SOLAR AND INFRARED FLUX MODULES

FASST can use direct measurements of shortwave and longwave fluxes at the surface as input if they are

available, but in many instances such data are unavailable. In these cases, FASST uses Shapiro's (1987, 1982, 1972) model to predict downwelling direct and diffuse shortwave irradiance at the surface based on standard surface meteorological observations. This Shortwave Radiation Module also predicts the upwelling shortwave irradiance based on the downwelling shortwave irradiance and the surface albedo parameterized in terms of the land surface type. The basic model approach involves dividing the atmosphere into k layers and parameterizing the reflectance, transmission, and absorption of each layer in terms of the solar zenith angle θ_o and the state of the atmosphere/clouds using the very extensive SOLMET database (NOAA 1979). The general form of the flux equations is:

$$I_{s\downarrow}^{k} = T_k I_{s\downarrow}^{k-1} + R_k I_{s\uparrow}^{k} \tag{1a}$$

$$I_{s\uparrow}^{k} = T_{k+1} I_{s\uparrow}^{k+1} + R_{k+1} I_{s\downarrow}^{k} . \tag{1b}$$

Layer k=0 is the top of the atmosphere. For operational use the atmosphere has been divided into three layers consistent with the concept of low, middle, and high clouds. An adding technique is used to account for multiple reflection between the different layers and the ground. T_k and R_k are parameterized in terms of the atmospheric and cloud conditions as follows:

$$R_k = \phi_k \rho_k + (1-\phi_k) r_k \tag{2a}$$

$$T_k = \phi_k \tau_k + (1-\phi_k) \tau_k \tag{2b}$$

$$\phi_k = W_f . \tag{2c}$$

Layer k cloud reflectance ρ_k, clear sky reflectance r_k, cloud transmission τ_k, clear sky transmission t_k, and cloud weighting factor W are parameterized in terms of the cosine of the solar zenith angle using the SOLMET data set. The fractional cloud amount f_k is obtained from the observations or climatology.

The downwelling longwave radiation is calculated using the ambient air temperature, an effective atmospheric emissivity, the cloud amount, and the cloud base temperature based on the cloud base altitude parameterized in terms of the cloud type. The clear sky downwelling atmospheric radiation originates mainly in the lower atmosphere (below altitudes of several kilometers) where the absolute humidity is relatively high. This component ($I_{ir\downarrow}^{clr}$) is calculated from

$$I_{ir\downarrow}^{clr} = \varepsilon_a \sigma T_a \tag{3}$$

where ε_a is the effective atmospheric emissivity, T_a is the ambient air temperature, and σ is the Stefan-Boltzmann constant. The effective emissivity is calculated from Wachtmann's (Hodges et al. 1983) modification of Idso's (1981) formulation based on the air temperature and the relative humidity. For cloudy skies the flux ($I_{ir\downarrow}^{cld}$) is given as

$$I_{ir\downarrow}^{cld} = c_l \chi_l + c_{eff}^{m} \chi_m + c_{eff}^{h} \chi_h \tag{4}$$

where c_l is the fractional low cloud amount, c_{eff}^{m} and c_{eff}^{h} are the effective middle and high cloud cover amounts based on the principle of random overlap, and $\chi_{(i,m,h)}$ (cloud irradiance factor) is a function of the cloud base altitude. The cloud base altitude, if not available from observations, has been parameterized in terms of season and latitude following the approach by Stowe et al. (1980) and London (1957). The upwelling longwave radiation is based on the surface temperature and the surface emissivity. The surface emissivity has been characterized in terms of the land surface type.

3 SNOW ACCRETION AND DEPLETION, AND MELTWATER OUTFLOW

The snow accretion-depletion module is a physically based approach to modeling snow melt, where the physics of water flow through snow are considered and the melt is driven by an energy budget at the snow surface. This module uses a novel approach to modeling that combines time stepping with analytic mathematical solutions (Albert and Krajeski, 1998). Snow accretion occurs when a snowfall amount is given in the input or when precipitation is given in the input and the input air temperature is below freezing. In the latter case the precipitation amount is converted to a snowfall amount. For modeling the movement of water through the snow, the effects of capillarity are taken as negligibly small compared to the effects of gravity (Colbeck, 1972), yielding the simplified form of Darcy's equation for water flow in snow:

$$U = \frac{\rho_w k_w g}{\mu_w} \tag{5}$$

where U is the volume flux of the water through the snow, ρ_w is the density of water, k_w is the relative permeability to water, g is the acceleration due to gravity, and μ_w is the viscosity of water. Under some circumstances this will be applicable to the entire snowpack, while modifications will be necessary under some conditions of layering. The effective permeability k to the water phase is taken to be

proportional to a power (n) of the effective water saturation S (Morel-Saytoux 1969, Colbeck 1972). The general applicability of the relationship $k \propto S^n$ is discussed in depth in Mualem (1978). The water volume conservation equation (Colbeck 1972) used states that the change in water volume flux with depth is equal to the change in water saturation with time. To make the problem tractable, the total pore volume n, the irreducible water saturation, and the effective permeability are assumed to be constant over each time step. These variables change slowly compared to the time scale with which mobile water moves through the snow. The general solutions to the volume flux equations are sums in space and time of each impulse of mobile water resulting from either snow melt or rain as governed by the boundary conditions, while maintaining the governing restrictions. The accuracy of the solution will depend on the time step of the available meteorological data, with hourly data proving accurate enough to give promising results, and finer temporal resolution data resulting in more accurate approximations of the exact solution. The full set of governing equations and more detail on the method can be found in Albert and Krajeski (1998).

Snow depth prediction equations are based on the form used by Jordan (1991), which in turn comes from Anderson (1973). Both Jordan's and Anderson's earlier model break the snow into layers based on age, density, and crystal structure, while here the simplicity of a uniform bulk snowpack is maintained. The user may input actual measured snow depths at whatever time frequency they are available. In any given time step, if there is a snow depth given, the module will use the given snow depth. If there is no measured snow depth given, the model will predict the rate of densification and adjust the snow depth accordingly. Also calculated with snow depth are the density of ice within the snowpack, the density of ice plus irreducible water saturation plus mobile water saturation, the total pore volume as a fraction of total volume, the pore volume excluding pore volume filled with immobile water when meeting irreducible saturation requirements as a fraction of total volume, and the SWE (snow water equivalent).

The snow refreezing algorithm uses a time-averaged value of temperature over the most recent period in which the snowpack is predicted to be less than isothermal, and a depth-averaged value of saturation, along with the bulk approximated thermal conductivity of snow, to calculate the depth of penetration of the refreezing front. Since these values are updated at every time step, the depth of penetration produced should be accurate enough.

In generating melt, the model currently uses a full surface energy balance to calculate the volume of runoff which will be generated during each time step. In general, the heat input at the top of the snow (I_{top}) is:

$$I_{top} = I_{s\downarrow}\left(1-\alpha_{top}\right) + I_{ir\downarrow} - I_{ir\uparrow} + I_{sen} + I_{lat} + I_{conv} \quad (6)$$

where I_s is the downwelling solar radiation, α_{top} is the surface albedo pertinent to shortwave radiation, $I_{ir\downarrow}$ is the downwelling longwave radiation, $I_{ir\uparrow}$ is the upwelling longwave radiation, I_{sen} is the sensible heat flux, I_{lat} is the latent heat flux, and I_{conv} is the convective heat flux. Solar radiation and albedo are taken as inputs obtained from either measurements or from the solar and infrared flux modules described above.

4 SOIL STRENGTH AND MOISTURE

The soil moisture module predicts dynamic changes in the physical properties of soils. These physical properties are then used to predict a soil strength measurement (cone index). The model predicts the cone index as a function of moisture migration through a layered media at discrete time and spatial intervals. The cone index calculation can be used to predict, for example, trafficability and maximum speed of wheeled or tracked vehicles.

The formulation relates *in situ* soil strength variations to the physical properties of the soil (i.e., soil type, moisture content, overburden pressure, and density of the soil). An empirical relationship between soil moisture by weight and the bearing capacity of the soils as given by Rating Cone Index rating is given by Equation 7:

$$RCI = \exp[a - b\ln(m)] \quad (7)$$

where RCI is the soil strength in terms of Rating Cone Index, a and b are coefficients specified for each USCS soil type, and m is moisture content (by weight) of soil. The volume of water in the soil at any time is determined with a water budget routine as given in Equation (8):

$$V_{w[t,d]} = V_{w[t-1,d]} + \partial V_{w[t,d]} \quad (8)$$

where t is time and d is depth. Given a multi-layer system as shown in Figure 1, the volume of water at each interval can be computed as given in Equation 9.

Equation 9 splits the computations into three parts. The first is for the change in the volume of water in the surface layer. The second part can be subdivided into multiple layers. The third computation represents the change in the volume of water in the n^{th} layer, where the drainage into the soil and out toward the water table is the only controlling factor. The Sellers et al. (1986) equation is

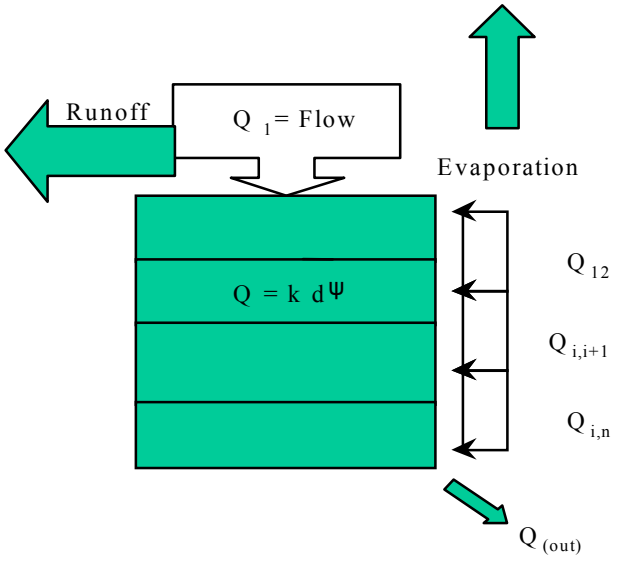

Figure 1: Multi-Layered Soil System

modified in Equation 9 with the term d to account for varying of the soil layers:

$$\partial V_{w[t,1]} \approx \partial V_{w[t-1,1]} - \left(Q_{(1,2)} \frac{d_1}{d_2} + E + R \right) \partial t$$

$$\partial V_{w[t,i]} \approx \partial V_{w[t-1,i]} - \left(Q_{(i,i-1)} \frac{d_{i-1}}{d_i} + Q_{(i,i+1)} \frac{d_i}{d_{i+1}} \right) \partial t \qquad (9)$$

$$\partial V_{w[t,n]} \approx \left(Q_{(i-1,i)} \frac{d_{i-1}}{d_i} - Q_{(out)} \right) \partial t$$

where Q is the flow through a layer, E is the evaporation at the near surface, and R is the runoff of the surface layer. The term Q accounts for flow between two consecutive layers of soil, including flow of water up or down in the system. The highest value of the flow is restricted to the saturated permeability of the soil. The flow is a function of pressure and permeability of the soil. The change in pressure between consecutive layers of soil controls the direction of the flow. The change in flow between layers is given in Equation 10 as a function of relative permeability and pressure:

$$\partial Q = 2K_r \left(\frac{\partial \psi_{i,i+1}}{d_i + d_{i+1}} + 1 \right) \qquad (10)$$

where K_r is the relative permeability and ψ is the bubbling pressure head.

The bubbling pressure can be measured in the field with a tensiometer and the saturated permeability with permeameter. The relationship between moisture content, bubbling pressure, and permeability is given by Clapp and Hornberger (1978). Although these equations are of agricultural and meteorological origin, civil engineers such as Rada et al. (1989) have converted the USDA classifications to USCS and used these relationships to address issues of road degradation at different times of the year.

The equation for the output flow Q_r from the lowest layer is given by Sellers et al. as:

$$Q_r = \sin(s) K_r \qquad (11)$$

where s is the slope of the terrain. Q_r assumes the r^{th} soil layer extends to the water table.

4.1 The Surface Layer

Occasionally the surface layer of soil may be a key modeling objective. This is particularly true when we consider short-term forecasts of less than one day in a region where dry weather has prevailed. When the precipitation events occur, slippery conditions on the surface reduce mobility considerably. To predict surface slippery conditions, a sorptivity term is introduced. Sorptivity is a measure of the surface layer's ability to absorb or de-absorb water. Computation of the sorptivity of the surface layer will define the amount of water the soil will take in over small increments of time. The equation for sorptivity as given by Clapp and Hornberger (1978) is shown in Equation 12 for a zero-pressure problem:

$$\Omega = \left(2 K_s \psi_s \theta s\right)^{1/2} (1 - W_i) \qquad (12)$$

where Ω is the sorptivity at zero surface pressure, and S is saturation. The sorptivity is related to the volume of water absorbed to the soil per unit time. Equation 12 expresses sorptivity, permeability, and time as a function of flow into the surface.

4.2 Evaporation Rate

A simple evaporation description has been implemented, following the equation:

$$E = 0.33(e_s - e_d) \cdot u_2^{0.76} \qquad (13)$$

where E is the evaporation rate, e_s is the vapor pressure at the surface, e_d is the saturation vapor pressure at the current air temperature, u_2 is the wind velocity at 2 m above the ground, h is the relative humidity, and e_a is the vapor pressure at the mean air temperature.

5 GROUND FREEZE/THAW MODULE

The ground freeze/thaw module assumes the temperature profiles are linear across the snow and ground layers, a reasonable approximation for naturally occurring conditions of interest. The model uses simple flux balance relations to evaluate the interface temperatures in terms of energy input and medium properties. The possible model layers (Fig. 2) are air, snow, frozen soil, and unfrozen soil. Snow may be absent. Heat fluxes through the layers are positive in the upward direction. The freezing front is at the base of the frozen soil and the top of the unfrozen soil, with temperature T_{fu}, which is taken to be zero (freezing point depression is neglected). The ground is assumed to cool gradually as the freezing season approaches, so that the surface layer is approximately 0°C when freezing finally commences and when snow accumulates. This means that the heat flux within the uppermost layer of soil is negligible when there is snow accumulation and/or freeze.

The energy input/output that drives the system constitutes the heat flux Q_a between the air and the surface, whether snow covered or bare soil. Q_a in turn consists of a conductive/convective mixing portion, plus a radiation portion:

$$Q_a = h_a \left(T_{sa} - T_a \right) + Q_{rad} \tag{14}$$

where Q_{rad} is the net radiation flux and T_a is the ambient temperature. The surface–atmosphere heat transfer h_a is expressed as

$$h_a = h_o + h_w W \tag{15}$$

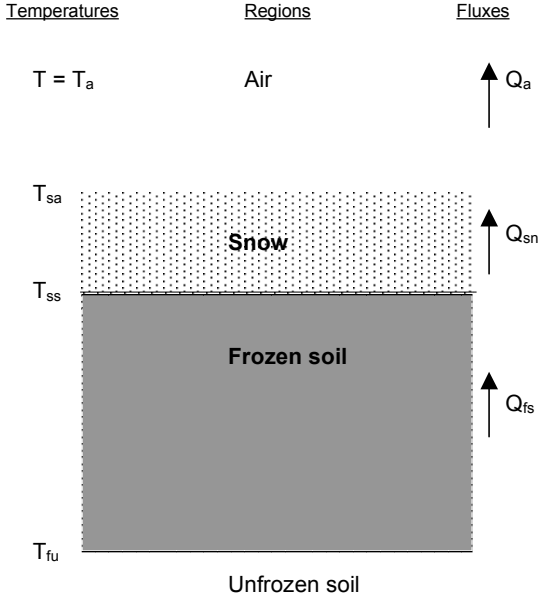

Figure 2: Model Notation for Interface Temperatures and Layer Fluxes

where W denotes the daily average wind speed (m/s). Based on field experiments, the coefficients h_o and h_w are taken to be 1.8 W/m^2 °C and 6.0 J/m^3 °C, respectively (Jordan, 1991). When snow is present, the fluxes in the snow and frozen soil are expressed as

$$Q_{sn} = \left(\frac{K_{sn}}{d_{sn}} \right) \left(T_{ss} - T_{sa} \right) \tag{16a}$$

and

$$Q_{fs} = \left(\frac{K_{fs}}{d_f} \right) \left(T_{fu} - T_{ss} \right) = \left(\frac{-K_{fs}}{d_f} \right) T_{ss} \tag{16b}$$

K_{sn} and K_{fs} are the thermal conductivities of the snow and frozen soil, respectively, d_{sn} is the depth of the snow, and d_f is the depth of the frozen soil. Assuming continuity of flux across the frozen soil–snow interface ($Q_{sn} = Q_{fs}$). leads to

$$T_{ss} = \left[\frac{1}{\left(\frac{K_{fs}}{K_{sn}} \right) \left(\frac{d_{sn}}{d_f} \right) + 1} \right] T_{sa} = B_{sa} T_{sa} \tag{17}$$

where B_{sa} denotes the expression in brackets. Continuity of fluxes across the snow–air interface ($Q_{sn} = Q_a$) leads to

$$T_{sa} = \frac{h_a T_a - Q_{rad}}{h_a + \left(K_{sn} / d_{sn} \right) \left(1 - B_{sa} \right)}. \tag{18}$$

Flux across the freeze front is not continuous. Above the freeze front it is equal to the rate at which energy is extracted into the atmosphere; below, it is assumed to be approximately zero. The difference is equal to the rate at which latent heat is supplied by the phase change process and is proportional to the freeze rate:

$$v_f = Q_{fs} / L \tag{19}$$

where L is the latent heat of fusion, and v_f is the freezing rate. Overall, the phase change rate is equal to the rate of penetration of either freeze or thaw (v_f or v_{th}). This series of equations can be used to solve for the rate of freezing. If the net surface flux Q_a is negative, i.e. the surface is *warming*, then no action is taken in the soil freezing calculations. This warming is assumed to produce some melt within the snow, as handled by the snow accretion-depletion module.

When there is no snow but freezing occurs, the first layer is frozen while the second is unfrozen. If thawing occurs, the first layer is unfrozen while the second is frozen. It is assumed that as the upper layer freezes or thaws, the lower layer is approximately isothermal at the phase change temperature. Thus, there is negligible conduction near the layer 1–layer 2 interface. That interface is at the phase change temperature $T_{fu} = 0°C$, and it advances downwards if there is any further freeze or thaw. Thus, it is possible to equate the flux across the air–layer 1 interface to the flux across the layer 1–layer 2 interface:

$$h_a(T_{sa} - T_a) + Q_{rad} = \frac{K_s}{d_s}(T_{fu} - T_{sa}) \tag{20}$$

where K_s and d_s are the thermal conductivity and thickness of the top soil layer, respectively. Solving for T_{sa}:

$$T_{sa} = \frac{h_a T_a - Q_{rad}}{h_a + K_s / d_s} \tag{21}$$

The flux across soil layer 1 is

$$Q_s = \left(\frac{-K_s}{d_s}\right) T_{sa} \tag{22}$$

and the phase change rate v_{pc} is proportional to it

$$v_{pc} = \pm \frac{Q_s}{L}. \tag{23}$$

When Q_s is positive, freezing progresses; when negative, thawing occurs.

The initiation of freezing for a snowless soil cannot occur until the soil temperature is near freezing. The heat storage in the soil is represented by a Cumulative Freeze Index (CFI) based either on data, if available, or on climatological conditions for the selected location. The climatological CFI is based on the timing between the first day the average temperature is below freezing and the first day frozen soil conditions are present. A daily CFI is computed from the climatological CFI, the daily average air temperature, the depth of the snow cover, a daily decay coefficient, and a snow reduction coefficient. Freezing cannot occur until the daily CFI is zero or greater. The onset of significant thawing cannot occur until there is no snow cover. When the flux to the atmosphere Q_a is positive and the soil is unfrozen, freeze is initiated. When it is negative and the soil is significantly frozen, then thaw is initiated. In either case, the rate of phase change (i.e. rate of freeze or thaw penetration) is simply Q_a/L since it is assumed that the underlying soil is at the phase change temperature. Based on the input from the soil moisture module when freezing begins, the algorithm locks in the soil moisture content of the frozen soil. When thaw is initiated, the algorithm assumes that the very first thaw layer is wet, at 90% saturation, at least for the purpose of calculating the thermal conductivity and sensible heat capacity. After the first day of thaw, should it continue, the ground freeze/thaw module accepts whatever thawed soil moisture value it receives as input.

During initiation of thawing, two factors can combine to promote excessive melting: 1) neglect of sensible heat (inherent in the quasi-static linear temperature profile assumption) and 2) the fact that soil thaw might occur after there has been a great deal of snow melt. When the initial thaw is especially rapid, a more accurate estimate of the rate is obtained by including sensible heat. For the test case pursued in the validation, neglecting sensible heat caused energy errors on the order of 50% in the first day or two of the seasonal collapse of the frozen layer. An estimate of the sensible heat change ΔH_s in the upper level of the soil based on a linear gradient between $T_{fu(=0°C)}$ at depth d_s and T_{sa} for a soil volumetric sensible heat capacity c_v is computed:

$$\Delta H_s = \tfrac{1}{2} c_v T_{sa} d_s \,. \tag{24}$$

The value of c_v is calculated by the program based on tabulated specific heats of water and typical soil minerals, given the soil volumetric moisture content. A portion of Q_a is absorbed by ΔH_s and does not contribute to thawing. Thus, equation (11) becomes

$$v_{th} = -(Q_a + \Delta H_s)/L \tag{25}$$

where v_{th} denotes the thaw rate.

6 SOLAR AND INFRARED FLUX MODULE COMPARISON WITH MEASURED DATA

The solar and infrared flux modules were tested using data from the Smart Weapons Operability Enhancement (SWOE) field program. The SWOE field programs were conducted during the fall of 1992 (Grayling, MI), the spring/summer of 1993(Yuma, AZ), and the winter/spring of 1994 (Grayling, MI). Hourly average values of the meteorological information were used to evaluate the flux models. During daylight hours, observations of the cloud cover were made on the hour from approximately 0700 to 1900 local time. It should be realized that the cloud amount might not be consistent with the average hourly average values of the measured solar flux. Since the exact time of

the cloud observations is unknown, it is not possible to use the one-minute observation that corresponds to the cloud amount. Cloud amount can have a significant impact on both the solar and infrared flux. In general, an increase in the cloud amount will decrease the solar flux and increase the infrared flux. Figure 3 is a comparison of the model-calculated total solar flux and the corresponding measured flux for a six-day period for the hours between 0700 and 1900 local from the Grayling I data set. The phasing and the amplitudes match fairly well for clear conditions. Differences occur mainly for cloudy conditions. The solar flux model does not require cloud optical depth information. The dependence on optical depth is implicit in the coefficients for transmission, reflectance, and the cloud weighting function.

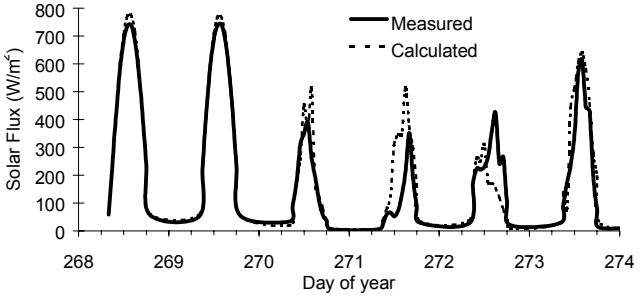

Figure 3: Comparison of Measured and Calculated Total Solar Flux for a Six-day Period for Grayling I. Only the Values of the Solar Flux when the Zenith Angle is less than 90 Degrees are Plotted

Most surface energy budget models, including FASST, utilize only the total solar flux. Figure 4 is a plot of the measured and computed downwelling longwave flux as a function of the fractional day of the year. There is good agreement between the measured and calculated longwave values.

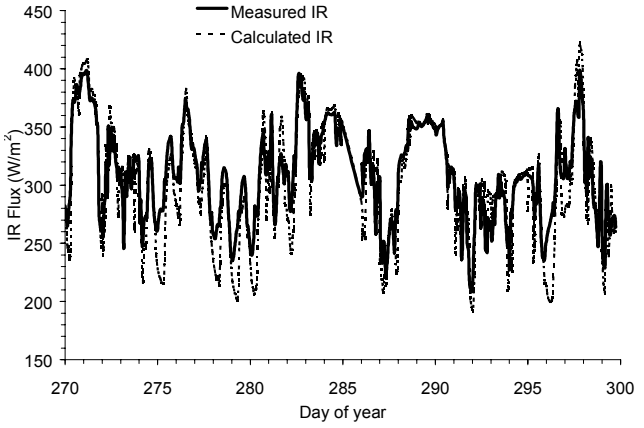

Figure 4: Comparison of Downwelling Measured and Computed Longwave Flux Based on the Grayling I Meteorological Observations

7 SNOW CALCULATIONS COMPARISON WITH FIELD DATA

Model results of the snow module are compared to field data obtained at the Sleepers River Research Watershed in northern Vermont in Figure 5. The water flux out of the snowpack is denoted by open circles, and the hourly model predictions by closed squares. For reference, the hourly air temperature is plotted at the top of the graph. The first five days were sunny, clear days with cooler nights, while the last five days included clouds and the passage of a storm front. In general, the model results agree well with measured lysimeter data.

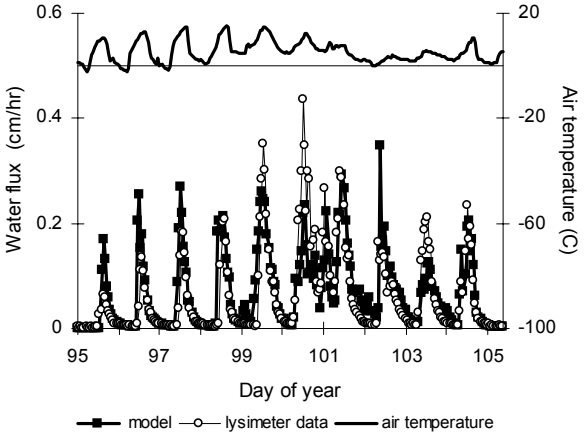

Figure 5: Comparison of Measured and Modeled Snowmelt Outflow During the Main Melt Season. The Measured Outflow is Field Data from a Snowmelt Lysimeter

The model predicts snow depth over time, in response to precipitation, settlement, and melt, as discussed above. In Figure 6 the measured and modeled snow depth over the course of the winter is depicted. In general the results compare well, although there are differences whose origin may be due to difficulties in discerning whether precipitation events are snow or rain (precipitation is usually reported as water equivalent; in the model, if the air temperature is less than 0.5°C, precipitation is assumed to be snow). The model results and measured snow depth show reasonable agreement. Future upgrades will be made to the model in terms of implementing improvements in the energy balance modeling and snow settlement.

8 FREEZE/THAW CALCULATIONS COMPARISON WITH FIELD DATA

The soil freeze/thaw module automatically calculates all volume fractions based on dry density and moisture content and then determines the soil thermal conductivities from these. No field measurements were taken of soil moisture content during thaw. Given that the thaw occurs

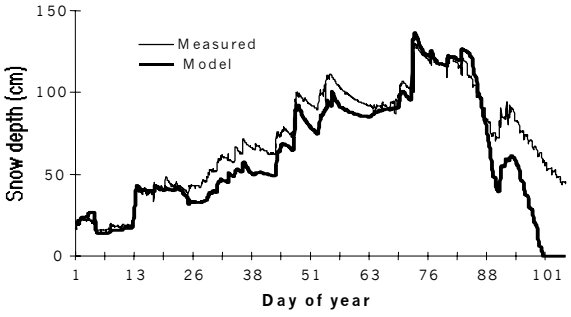

Figure 6: Measured and Modeled Snow Depths over the Course of the Winter

directly after snow melt, with a frozen sublayer that prevents drainage, it is assumed that the thawed soil layer is approximately 90% saturated. Figure 7 compares the predicted depth of freeze with the observed depth of freeze over the course of a winter season.

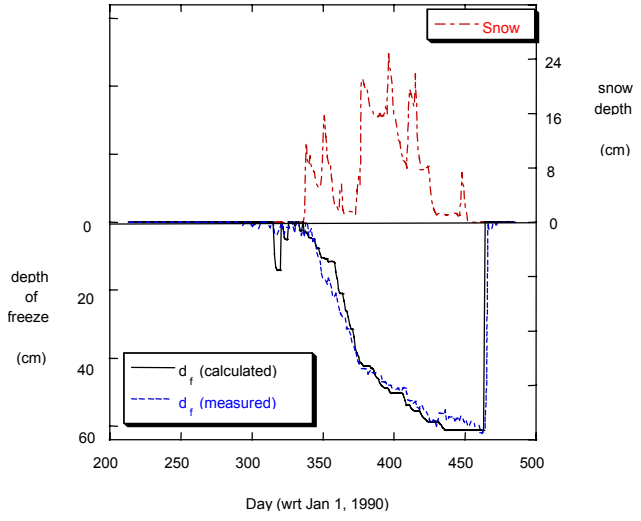

Figure 7: Comparison of Measured and Modeled Frost Depth over the Course of the Winter, with Snow Depth Shown for Reference

There is remarkably good agreement between the calculated and measured depths of freeze, with the largest error during a transient early season episode before any snow had accumulated (Figure 7). The pattern and magnitude of frost penetration is portrayed faithfully, as is the timing of the ultimate collapse of the frost layer at the end of the season.

9 SOIL MOISTURE CALCULATIONS COMPARISON WITH FIELD DATA

A limited field test was conducted to compare predicted versus measured cone index readings. The site was located at Fort Leonard Wood, Missouri. The site included a weather station located on grass-covered lean clay. The slope was 1 percent. Figure 8 illustrates the predicted moisture content for the top 3 cm of soil versus the measured moisture content by weight. The measured readings were found to compare favorably with the predicted values. The subsurface readings were taken between 7 and 12 cm. Figure 9 illustrates these results. The data appeared to oscillate; however, the predictions were near the measured readings. In this study we located the water table at 40 cm, which may have attributed to the oscillations in soil strength. Current efforts in the model include linking soil temperature effects more closely with soil moisture and further development of the soil moisture algorithm.

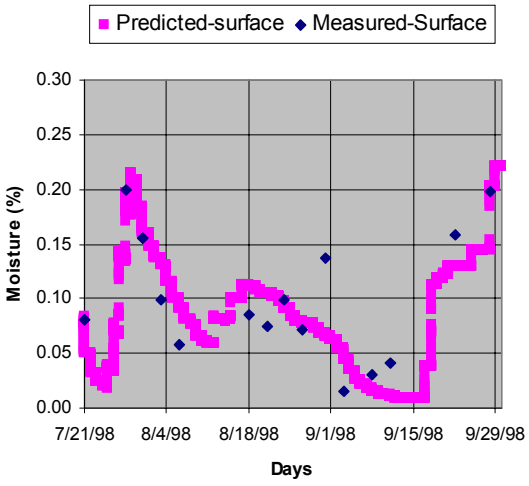

Figure 8: Predicted vs. Measured Moisture Content for Surface Layer

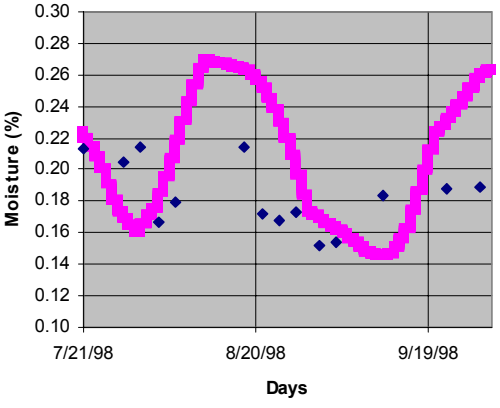

Figure 9: Predicted vs. Measured Moisture Content for 7- to 12-cm Layer

10 CONCLUSION

Initial evaluation of some of the components of the Fast All-Seasons Soil State model show good agreement with measured field data. At the present time, there is no

existing data set that contains all of the data at a single location that experiences winter (snow/ice) as well as summer conditions, so the model components are compared to data available from a variety of locations over relatively small time periods. In ongoing work, a year-round complete data set will be developed that contains all of the components necessary to fully evaluate the model. In addition, further model development and improvement are currently underway for many model components, including soil temperature. Model development is continuing with an aim at computational efficiency, so that year-round predictions of the state of the ground can be possible using limited computer resources, for example personal computers.

11 ACKNOWLEDGMENT

This work is funded by Department of the Army work units AT42 Model for all-seasons soil strength predictions and AT42 -TO17.

REFERENCES

Albert, M., and G. Krajeski. 1998. A fast, physically based point snowmelt model for use in distributed applications. *Hydrological Processes* 12: 1809-1824.

Anderson, E.A. 1973. National Weather Service River Forecast System Snow Accumulation and Ablation Model. NOAA Technical Memorandum NWS 17, National Oceanic and Atmospheric Administration, Bethesda, MD.

Clapp, R.B., and G.M. Hornberger. 1978. Empirical equations for some soil hydraulic properties. *Water Resource Research* 14: 601-604.

Colbeck, S.C. 1972. A theory of water percolation in snow. *Journal of Glaciology* 11(63): 369-385.

Hodges, D.B., G.J. Higgins, P.F. Hilton, R. Shapiro, C.N. Touart, and R.F. Wachtmann. 1983. Final tactical decision aid (FTDA) for infrared 8-12 micron systems. Technical backgrounds. Scientific Report No. 5, Systems and Applied Sciences Corporation. Report AFGL-TR-83-0022, Air Force Geophysics Laboratory.

Idso, S.B. 1981. A set of equations for full spectrum and 8-14 micron and 10.5-12.5 micron thermal radiation from cloudless skies. *Water Resources Research* 17: 295-304.

Jordan, R. 1991. A one-dimensional temperature model for a snow cover: Technical documentation for SNTHERM.89. Special Report 91-16, U.S. Army Corps of Engineers, Cold Regions Research and Engineering Laboratory, Hanover, NH.

London, J. 1957. A study of the atmospheric heat balance. Final Report, Contract AF19(122)-165 (AFCRC-TR-57-287), New York University {ASTIN 117227}.

Morel-Seytoux, H.J. 1969. Introduction to flow of immiscible liquids in porous media. In *Flow through porous media*, ed. R.J.M. De Wiest, 455-516. New York: Academic Press.

Mualem, Y. 1978. Hydraulic conductivity of unsaturated porous media: Generalized macroscopic approach. *Water Resources Research* 14:. 324-334.

NOAA. 1979. SOLMET VOL 2, Hourly solar radiation-surface meteorological observations, Final Report. D-9724, National Climatic Center, Asheville, NC.

Rada, G.R., C.W. Schwarz, and W.M. Witczak. 1989. Prediction of damage to secondary roads. *Journal of Transportation Engineering* 115: 4.

Sellers, P.J., Y. Mintz, Y.A. Sud, and A. Dalcher. 1986. A simple biosphere model (SIB) for use within general circulation models. *Journal of Atmospheric Sciences* 43: 505-531.

Shapiro, R. 1987. A simple model for the calculation of the flux of direct and diffuse solar radiation through the atmosphere. AFGL-TR-0200, U.S. Air Force.

Shapiro, R. Simple model for the calculation of the flux of solar radiation through the atmosphere. *Appl. Opt.* 11: 760-764.

Shapiro, R. 1982. Solar radiative flux calculations from standard surface meteorological observations. AFGL-TR-82-0039, U.S. Air Force.

Stowe, L.L., H. Jacobowitz, and V.R. Taylor. 1980. Reflectance characteristics of earth and cloud surfaces as measured by the ERB scanning channels on the Nimbus-7 satellite. In *Proceedings International Radiation Symposium,* 430-432, Fort Collins, Colorado.

AUTHOR BIOGRAPHIES

MARY R. ALBERT is a Research Mechanical Engineer in the Geophysical Sciences Division of the Engineer Research and Development Center (ERDC) Cold Regions Research and Engineering Laboratory (CRREL) in Hanover, NH. She received her B.S. in Mathematics from Penn State, M.S. in Engineering Sciences from Dartmouth, and Ph.D. in Applied Mechanics from the University of California at San Diego. She is president of the Eastern Snow Conference and a member of the I.G.S., A.G.U., and A.S.M.E. Her fields of study are snow physics, heat and mass transport processes, and numerical analysis. Mary's email address is <malbert@crrel.usace.army.mil>.

GEORGE G. KOENIG is a Physical Scientist at the Engineer Research and Development Center (ERDC) Cold Regions Research and Engineering Laboratory (CRREL) in Hanover, NH. He received a B.S. degree in Physics from the State University College at Oneonta, NY, an M.S. in Aeronomy from the University of Michigan, and a Ph.D. in

Atmospheric Science from the University of Utah. Dr. Koenig retired as Lt. Col. from the Air Weather Service (USAF). His present research work involves the development of physics-based energy budget models for multispectral synthetic scene generation and modeling of passive and active MMW systems to detect in-cloud icing potential. His e-mail address is <gkoenig@crrel.usace.army.mil>

GEORGE L. MASON is a Research Civil Engineer for the Engineer Research and Development Center (ERDC), Mobility Systems Division at Waterways Experiment Station, Vicksburg, MS. He received his BSCE and MSCE from Mississippi State University and his Ph.D. from Rennselaer Polytechnic Institute. He is a licensed Professional Engineer in the state of MS. He is a member of MORS, MES, SISO, and ISTVS. His email address is <masong@wes.army.mil>.